

Quantum metrology with partially accessible chaotic sensors

Harshita Sharma ,^{1,*} Sayan Choudhury ,^{2,†} and Jayendra N. Bandyopadhyay ,^{1,‡}

¹*Department of Physics, Birla Institute of Technology and Science Pilani, Pilani Campus, Vidya Vihar, Pilani, Rajasthan 333031, India.*

²*Harish-Chandra Research Institute, a CI of Homi Bhabha National Institute, Chhatnag Road, Jhunsi, Allahabad 211019, India*

Most quantum metrology protocols harness highly entangled probe states and globally accessible measurements to surpass the standard quantum limit. However, it is challenging to satisfy these requirements in realistic many-body sensors. We demonstrate that both of these constraints can be overcome in quantum chaotic sensors. Crucially, we establish that even in the presence of partial measurement accessibility, chaotic dynamics enables initial unentangled states to exhibit Heisenberg scaling of the quantum Fisher information, I_α with time. In the weakly chaotic regime, we identify spin-coherent states placed at the edge of the regular islands in the mixed classical phase space as optimal initial states for enhanced sensitivity. On the other hand, in the strongly chaotic regime, I_α is insensitive to the choice of the initial state. Notably, quantum-enhanced sensitivity is achieved even when a very low fraction ($\sim 5\%$) of the qubits are accessible. These results establish quantum chaos as a robust resource for quantum-enhanced sensing under realistic accessibility constraints on accessibility.

Introduction: In classical systems, the maximum achievable measurement precision for estimating an unknown parameter θ is governed by the Cramér-Rao bound [1, 2]: $\Delta\theta \geq 1/\sqrt{I_c}$, where I_c is the Fisher information [3, 4]. We note that I_c typically scales linearly with the number of classical resources N and the duration of the protocol, t . These considerations lead to the standard quantum limit (SQL), $\Delta\theta \geq 1/\sqrt{Nt}$, which bounds the precision of classical measurements [5, 6]. Intriguingly, this limit can be surpassed by harnessing genuinely quantum resources, such as entanglement [7–12], spin squeezing [13–18], and coherence [19–22]. Consequently, quantum systems have emerged as natural candidates for metrological applications [23, 24], including gravitational-wave detection [25–28], particle physics experiments [29], navigation [30], fundamental physics [31, 32], precision timekeeping [33], and magnetometry [34–36]. In this framework, the ultimate achievable precision is governed by the quantum Fisher information (QFI), I_α . The celebrated Heisenberg limit is achieved when the QFI scales quadratically both N and t : $I_\alpha \propto N^2 t^2$ [37]. Several works have explored routes such as non-linearity [38–46] and quantum criticality [44, 47–58] to reach and even surpass this limit. However, the preparation and preservation of these states in many-body systems remains experimentally challenging. Furthermore, the optimal protocols for achieving the highest measurement precision often require globally accessible measurements, which are experimentally unfeasible. However, partial access to the system can lead to a drastic decrease in the QFI and, consequently, the sensing capabilities. These challenges motivate the need to devise mechanisms to enhance QFI that do not depend on the careful preparation of probe states or global accessibility.

Intriguingly, some recent works have demonstrated that information scrambling in collective spin systems can be harnessed to circumvent the state preparation challenge [59–65].

Notably, quantum chaotic systems can be employed to achieve increased sensitivity even when the initial state is a product state [66, 67]. Remarkably, these protocols remain robust in the presence of noise [68], thereby providing a striking example of resilient designs [69]. Concurrently with these developments, some recent works have focused on the development of optimized measurement protocols that addresses the partial accessibility challenge in quantum critical and light-matter coupled systems [70–74]. These considerations naturally raise an intriguing question: is it possible to harness chaos for *resilient* quantum-enhanced sensing in the presence of partial access measurements?

In this Letter, we present an affirmative answer to this question by demonstrating that long-range interacting chaotic systems provide a route for *resilient* quantum-enhanced sensing even when a very small fraction of the system is accessible. We model the sensor as the paradigmatic quantum kicked top (QKT), where the strength of the chaoticity can be controlled by tuning the non-linearity [75]. This system serves as a powerful resource for quantum sensing, when globally accessible measurements can be performed [66]. Strikingly, we demonstrate that chaotic dynamics enables even the development of a large QFI, even when a small fraction ($\sim 10\%$) of the system is accessible. We find that, for a moderately chaotic case, the QFI under partial accessibility exhibits a strong dependence on the choice of initial state. In particular, initial coherent states, localized at the edges of regular islands, exhibit a larger QFI at late times and achieve Heisenberg scaling in time. In the strongly chaotic regime, there is no initial state dependence and the temporal growth of I_Q in the partially accessible QKT mirrors that of the fully accessible QKT. We conclude that quantum chaotic sensors retain their resilience in the presence of partial accessibility, thereby providing a robust platform for quantum metrology.

Model and Diagnostics: We examine the dynamics of a periodically driven system of N qubits interacting via infinite-range interactions described by:

$$H(t) = \frac{\kappa}{N} \sum_{i,j} s_i^y s_j^y + \frac{\alpha}{\tau} \sum_i s_i^z \sum_{n=-\infty}^{+\infty} \delta(t - n\tau), \quad (1)$$

* harshita.research25@gmail.com

† sayanchoudhury@hri.res.in

‡ jnbandyo@gmail.com

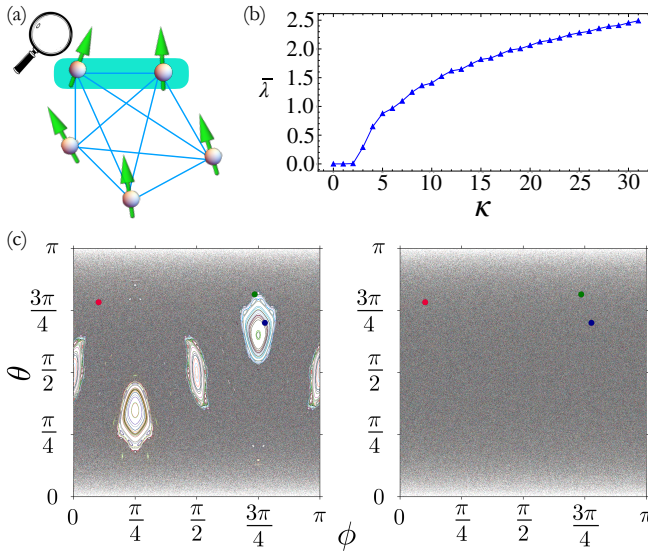


FIG. 1. (a) A schematic illustration of the “all-to-all” interacting quantum kicked top model under partial access. (b) The phase space averaged Lyapunov exponent that captures the sensitive dependence on initial conditions. The average is performed over 40,000 trajectories evolved over 50,000 drive periods. (c) The phase space map for (a) $\kappa = 3.0$ and (b) $\kappa = 30.0$. Different initial coherent states $|\theta, \phi\rangle$ are marked: non-equatorial island $|2.20, 2.44\rangle$ (blue circle), chaotic sea $|2.46, 0.32\rangle$ (red circle), and an edge state $|2.56, 2.31\rangle$ (green circle). Details regarding map generation are discussed in Appendix A. In the case of $\kappa = 30.0$, the system is strongly chaotic, and hence there are no distinguishable regular islands.

where $s_i^a = \frac{1}{2}\sigma_i^a$, where σ_i^a represent the standard Pauli matrices. the first term of the Hamiltonian describes the qubit-qubit interactions, and the second term describes a kick-induced rotation of each qubit about the z -axis. We set the kicking period $\tau = 1.0$ and $\alpha = \frac{\pi}{2}$ for the rest of this work. Due to the collective nature of the system, the Floquet unitary describing the stroboscopic time evolution of the system is represented by:

$$U = e^{-i\frac{\kappa}{2J}J_y^2}e^{-i\alpha J_z} \quad (2)$$

$J_i^a = \sum_i \sigma_i^a$ are the collective angular momentum operators satisfying $[J_i, J_k] = i\epsilon_{ikl}J_l$ and $j = N/2$. We note that time-evolution under this Floquet unitary has been studied widely in the context of the celebrated quantum chaotic model of the QKT [75, 76]. Before proceeding further, it is instructive to examine the dynamics of the QKT in the (semi)classical limit ($j \rightarrow \infty$) In this regime, the phase-space averaged Lyapunov exponent can be employed to characterize its chaoticity of the system. Our results are shown in Fig. 1 (b). It is evident that the system is not chaotic when $\kappa < 2$; it begins to exhibit chaotic behavior as κ increases. This is reflected in the phase space portraits of the system shown in Fig. 1 (c). In the moderately chaotic regime ($\kappa = 3$), the system hosts a mixed phase space with co-existing regular islands and chaotic regions. However, in the strongly chaotic large κ regime ($\kappa = 30$), the regular islands completely disappear. In this work, we analyze the efficacy of the sensor in both of these regimes.

We characterize the sensing capabilities of the QKT sensor by computing the QFI [66]:

$$I_\alpha(t) = 2 \sum_{nm} \frac{|\langle \psi_m | \partial_\theta \rho_\theta | \psi_n \rangle|^2}{p_n + p_m}, \quad (3)$$

where ∂_θ denotes differentiation with respect to the parameter θ , p_n and p_m are eigenvalues of the the mixed state ρ with eigenvectors $|\psi_n\rangle$ and $|\psi_m\rangle$, respectively, and the condition $p_n + p_m \neq 0$ is satisfied [77–79]. As noted earlier, I_α quantifies the precision with which a parameter, say θ , encoded in a quantum state can be estimated by providing an upper bound on the Fisher information for all possible generalized measurements [77]: $\Delta\theta_{CR} \geq \Delta\theta_{QCR} = 1/\sqrt{I_q}$ [80–82]. We note that the QFI is also used as a diagnostic for multipartite entanglement [83–85] and for detecting quantum phase transitions [54, 86–88]. We note that for a pure state ψ_θ , the general formula for the QFI simplifies to $I_\alpha(t) = 4(\langle \partial_\theta \psi_\theta | \partial_\theta \psi_\theta \rangle - |\langle \partial_\theta \psi_\theta | \psi_\theta \rangle|^2)$. In the case of partial accessibility however, we compute I_α (Eq. 3) for the reduced density matrix, ρ_Q corresponding to the accessible Q qubits of the N -qubit systems. The procedure for calculating ρ_Q is explicitly provided in Appendix B. In the rest of this work, we focus on the local estimation of α .

Results: We now proceed to investigate the behavior of the QFI for the QKT sensor composed of $N = 1000$ qubits ($j = 500$), both in the moderately chaotic ($\kappa = 3$) and the strongly chaotic ($\kappa = 30$) regime. We analyze the time-evolution of the system prepared in unentangled SU(2) spin-coherent states: [89–91]:

$$|\theta, \phi\rangle = e^{i\theta(J_x \sin \phi - J_y \cos \phi)} |j, j\rangle \quad (4)$$

In the moderately chaotic regime, the QFI exhibits a strong initial state dependence [66]. To illustrate this, we have examined the dynamics of the system for 3 different initial states from the mixed phase space as shown in Fig. 1: a non-equatorial island state $|2.20, 2.44\rangle$, chaotic sea state $|2.46, 0.32\rangle$, and green for edge state $|2.56, 2.31\rangle$. These states are represented in blue, red, and green colors respectively, in all the figures.

The time-evolution of the QFI in this regime for different subsystem sizes Q , ranging from $Q = 5$ to $Q = 500$ is shown in Fig. 2 (a)-(h). The case of global accessibility is also shown for comparison in Fig. 2(i). We note that at early times, an initial state corresponding to the chaotic region exhibits the largest QFI value; however, at later times, it is overtaken by the edge state. For smaller values of Q , the QFI fluctuates significantly for different initial states. As the number of accessible qubits is increased however, these fluctuations are suppressed. Crucially, the dependence of the QFI on the initial states persists even when we increase the number of accessible qubits Q . This observation highlights the metrological advantage of chaotic and edge states over initial regular island states, even under partial access.

For subsystem sizes up to 50% accessibility, the QFI exhibits robust scaling with time, approximately resembling

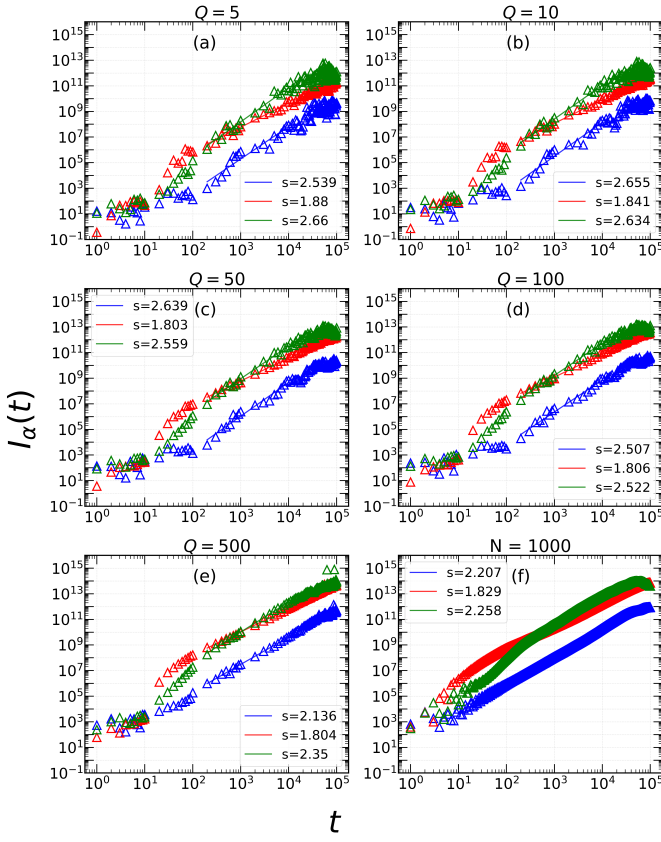


FIG. 2. Scaling of the QFI, I_α , is presented as a function of time t , for $\kappa = 3.0$ and different subsystem access Q , out of a total of $N = 1000$ qubits. Each panel shows the QFI for three different initial coherent states: a non-equatorial island state $|2.20, 2.44\rangle$ (blue), a state at the chaotic sea $|2.46, 0.32\rangle$ (red), and an edge state $|2.56, 2.31\rangle$ (green). At sufficiently later times, the edge state exhibits the highest QFI, followed closely by the chaotic sea state. Importantly, even in only 5% access, the QFI for the edge state nearly reaches the same order of magnitude as the full access case. The QFI vs time plots for more initial states are shown in Appendix C.

the fully accessible case. We note that the Ehrenfest time $t_E \simeq \ln(2J)/\lambda_E$ and the Heisenberg time $t_H \simeq J/3$ are characteristic time scales for the quantum dynamics of the QKT. We find that in the time interval $t_H < t \leq 10^4$, the QFI becomes superextensive, and the scaling exponent lies in the range $s \simeq [1.803, 2.719]$, indicating quantum-enhanced sensitivity. Moreover, the actual value of the QFI increases as Q is increased, in accordance with expectations. However, for the edge state, the QFI nearly reaches the same order as the full accessible case with as little as 5% access at later times. On the other hand, the overall growth of the QFI for all initial states with 50% access closely follows the global access situation for $\kappa = 3.0$.

The dependence of QFI with different subsystem sizes Q is shown in Fig. 3 for three representative times, where Q is varied from 1 to 900 qubits. At early times, the chaotic initial state yields the highest QFI for different subsystem sizes. At later times however, the difference between the QFI corre-

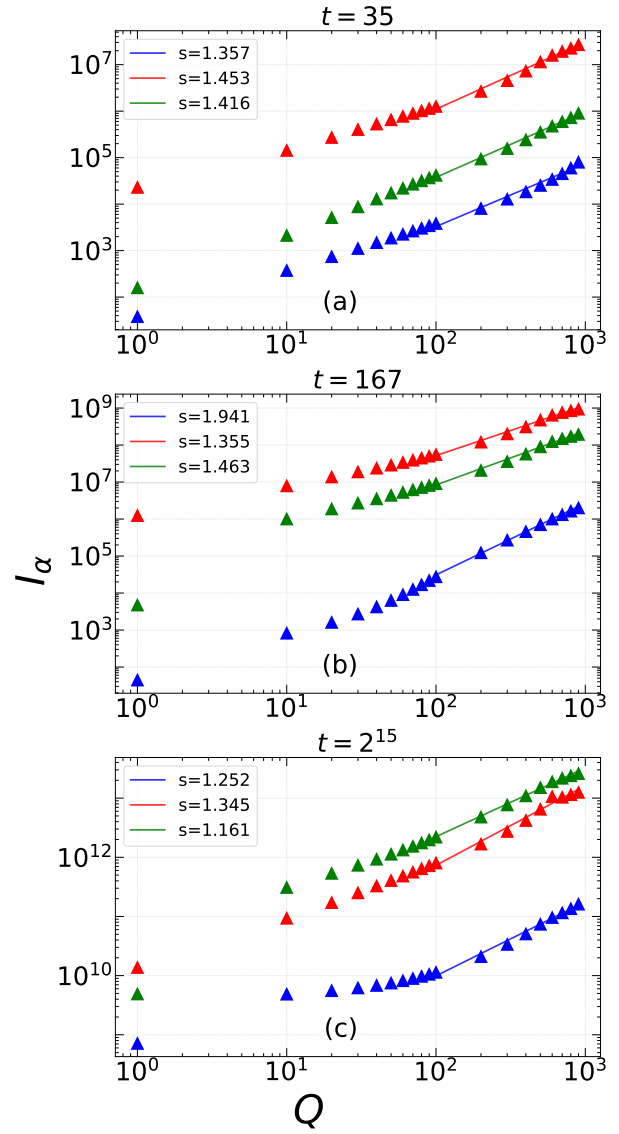


FIG. 3. Scaling of the QFI is shown as a function of the subsystem size Q for $\kappa = 3.0$ and at three different times : (a) $t = t_E = 35$, the Ehrenfest time for the edge state. (b) $t = t_H = 167$, the Heisenberg time of the system. (c) $t = 2^{15}$, a much later time $t \gg t_H$. With time evolution, the separation between the QFI of the initial chaotic and edge states reduces. Eventually, the QFI of the edge state surpasses that of the chaotic state and reaches its highest QFI value. A transition in QFI scaling is observed starting from $Q = 100$. However, at short times, the chaotic initial states provide the larger QFI values and hence the best candidates for sensing. QFI vs Q plots for more initial states are shown in Appendix C.

sponding to the chaotic and edge states reduces, and eventually, the edge state overtakes the chaotic state. A noticeable change in the QFI scaling is observed from $Q = 100$ as seen in Fig. 3(b) and (c). These results suggest that, although the scaling of the QFI is sub-Heisenberg, it still exhibits a superextensive scaling for measurements involving at least a 10% access to the total system.

For strong chaos with $\kappa = 30.0$, the system rapidly loses the

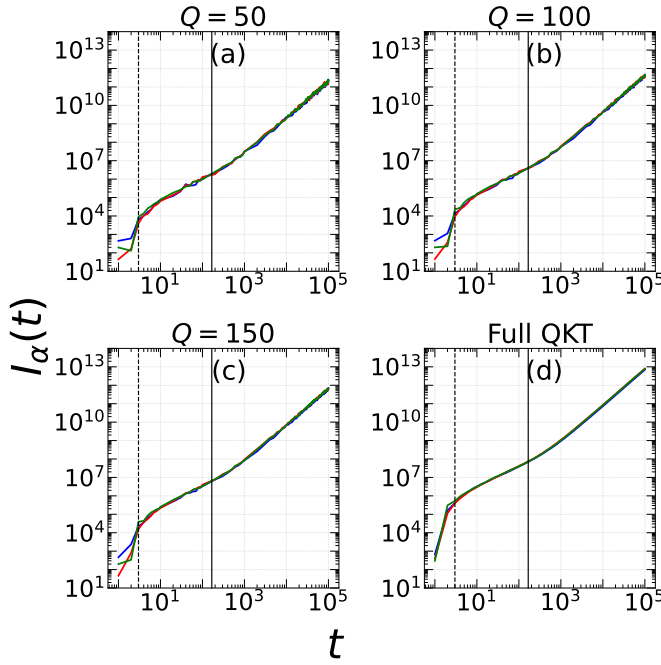


FIG. 4. Scaling of the QFI as a function of time t is shown at $\kappa = 30.0$ and for three different subsystem sizes: (a) $Q = 50$ qubits. (b) $Q = 100$ qubits. (c) $Q = 150$ qubits. (d) Fully accessed case with a total of 1000 qubits. The dotted line represents the Ehrenfest time $t_E = 3$ and the solid line represents the Heisenberg time $t_H = 167$. The trends of the QFI with time for the partially accessible case behave the same as the fully accessible QKT for the large value of the chaoticity parameter κ .

memory of its initial conditions, and the QFI does not exhibit any systematic initial state dependence [66]. This behavior persists even when only partial access to the system is available. Figure 4 provides evidence that the growth of the QFI for different subsystem sizes $Q = 50, 100, 150$ is almost the same as the fully accessible case for strong chaos. In the partially accessible case, the QFI exhibits slight irregularity prior to the Ehrenfest time t_E , and after that, the QFI displays the same memoryless nature as the fully accessible case. Finally, we note that while the temporal scaling of the QFI differs across the three regimes: $t < t_E$, $t_E < t < t_H$, and $t > t_H$, the qualitative behavior of the QFI growth with the magnitude of QFI increasing systematically as more qubits are accessed. The QFI scaling is super-Heisenberg till $t = t_E$, superextensive for $t_E < t < t_H$ and near Heisenberg for $t > t_H$.

Finally, we characterize the sensing capabilities of the system for various amounts of partial accessibility. To this end, we examine the ratio of the QFI with partial access I_{α_Q} , to that of the fully accessible case I_{α_N} , for any given initial coherent state; we dub this measure ‘Fractional QFI’. Fig. 5 shows the dependence of the fractional QFI on the fractional accessibility Q/N at three characteristic times: $t = t_E, t_H$, and $t \gg t_H$ for $\kappa = 3.0$ and 30.0 . A transition in slope is observed around $Q/N = 0.1$. The scaling for both $\kappa = 3.0$ and $\kappa = 30.0$ beyond this fractional access value (0.1) is super-extensive. Thus, access to about 10% of the total qubits

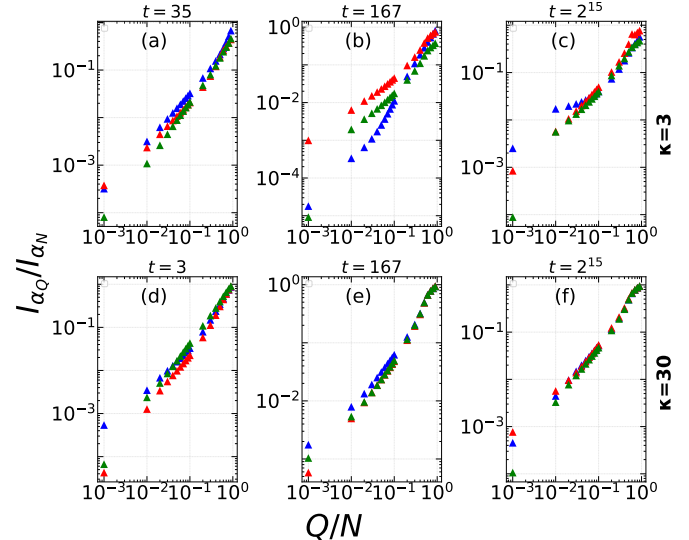


FIG. 5. Fractional QFI versus fractional access Q/N are shown for $\kappa = 3.0$ and 30.0 at different times. Panels (a)-(c) are for $\kappa = 3.0$ case and (d)-(f) are for $\kappa = 30.0$ case. A transition in the slope is observed around $Q/N = 0.1$ for both the cases.

is sufficient to extract a substantial amount of information about the encoded parameter, particularly during early time evolution.

Summary and Outlook: In this Letter, we have demonstrated that long-range interacting chaotic spin systems serve as quantum-enhanced sensors, even under partial accessibility. Remarkably, even without global access, the QFI still exhibits Heisenberg scaling with time, showing that chaos-assisted metrological enhancement remains robust under realistic measurement constraints. This feature is particularly relevant for experimental implementations, where global access is often impractical and local measurements are employed instead. We note that the QKT has been realized in a variety of platforms including superconducting qubit processors [92], ultracold atomic systems [93], and NMR platforms [94], thereby making our predictions verifiable in near-term experiments.

There are several avenues for future work. A natural extension of this work would be to examine the resilience of these partially accessible chaotic sensors in the presence of decoherence. Furthermore, it would be intriguing to develop quantum control protocols to further enhance the sensing capabilities of this system. Finally, it would be interesting to extend these studies to other kinds of resilient quantum sensors, such as those based on projected ensembles [69].

Acknowledgments: H.S. and J.N.B. acknowledge the Department of Science and Technology (DST) for providing computational resources through the FIST program (Project No. SR/FST/PS-1/2017/30). SC acknowledges funding under the Government of India’s National Quantum Mission grant numbered DST/FFT/NQM/QSM/2024/3.

Appendix A: Phase Map

The classical phase-space map can be obtained from the stroboscopic Heisenberg equations of motion for the generators, $X_i = \frac{J_i}{j}$ in the limit $j \rightarrow \infty$. For the Quantum Kicked Top (QKT) Hamiltonian, phase map is generated by the following equations:

$$\begin{aligned} X' &= (X \cos \alpha - Y \sin \alpha) \cos(\kappa(X \sin \alpha + Y \cos \alpha)) + Z \sin(\kappa(X \sin \alpha + Y \cos \alpha)) \\ Y' &= X \sin \alpha + Y \cos \alpha \\ Z' &= -(X \cos \alpha - Y \sin \alpha) \sin(\kappa(X \sin \alpha + Y \cos \alpha)) + Z \cos(\kappa(X \sin \alpha + Y \cos \alpha)) \end{aligned}$$

Appendix B: Reduced Density Matrix

The initial states used for simulation are the SU(2) spin-coherent states of the form :

$$|\psi\rangle = |j, \theta, \phi\rangle = |\theta, \phi\rangle = e^{i\theta(J_x \sin(\phi) - J_y \cos(\phi))} |j, j\rangle$$

These initial states can be expressed in the Dicke basis:

$$|\psi\rangle = \sum_{k=0}^N c_k |D_N^{(k)}\rangle \quad (\text{B1})$$

Now the Dicke states $|D_N^{(k)}\rangle$, which are completely symmetric N -qubit states of k up-spins and $N - k$ down-spins, can be written in the bipartite form as [95, 96] :

$$|D_N^{(k)}\rangle = \sum_{l=0}^Q \sqrt{\frac{\binom{Q}{l} \binom{N-Q}{k-l}}{\binom{N}{k}}} |D_Q^{(l)}\rangle \otimes |D_{N-Q}^{(k-l)}\rangle \quad (\text{B2})$$

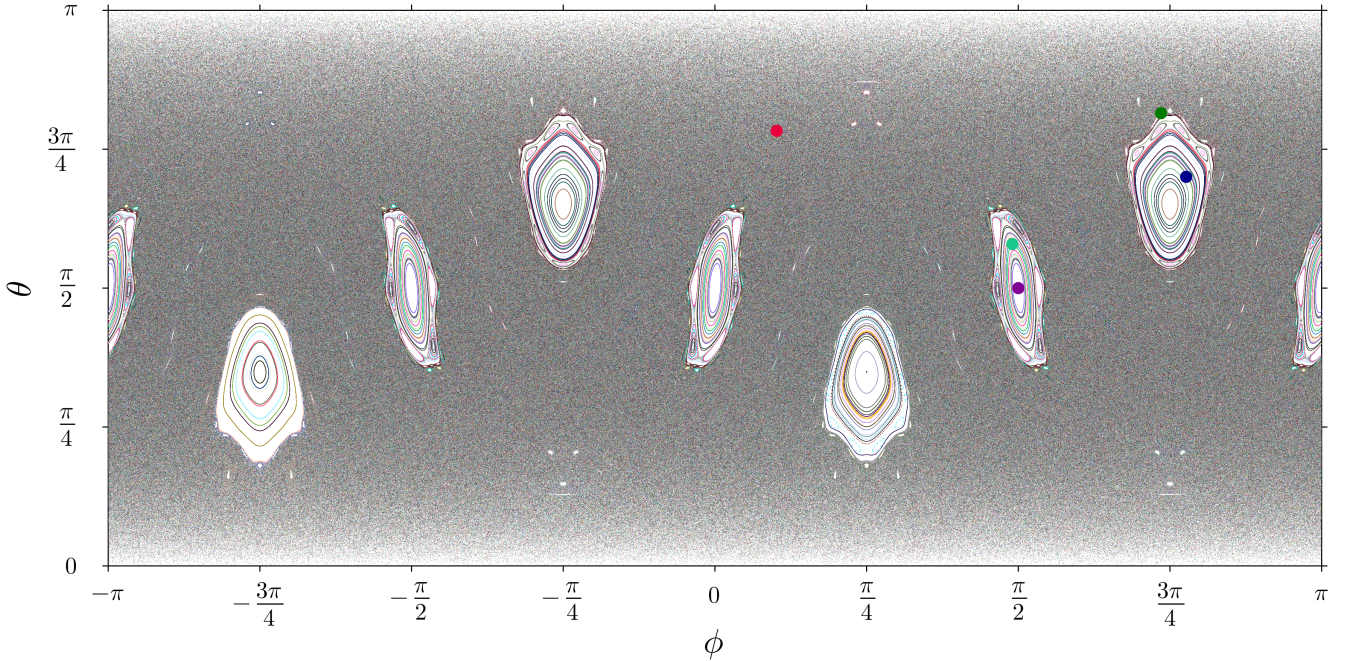


FIG. 6. Different initial coherent states $|\theta, \phi\rangle$ are marked: equatorial $|\pi/2, \pi/2\rangle$ (purple circle) and $|1.82, 1.54\rangle$ (limegreen circle), non-equatorial $|2.20, 2.44\rangle$ (blue circle), chaotic sea $|2.46, 0.32\rangle$ (red circle), and an edge state $|2.56, 2.31\rangle$ (green circle). The color scheme of the different plots for these initial states will be maintained as mentioned here.

Here we consider the bipartition into blocks of Q and $N - Q$ spins. The Q block has l up-spins and block $N - Q$ has $k - l$ up-spins. From Eqs. (B1) and (B2) we get:

$$\begin{aligned} |\psi\rangle &= \sum_{k=0}^N \sum_{l=0}^Q c_k \sqrt{\frac{\binom{Q}{l} \binom{N-Q}{k-l}}{\binom{N}{k}}} |D_Q^{(l)}\rangle \otimes |D_{N-Q}^{(k-l)}\rangle \\ &= \sum_{l=0}^Q \sum_{r=0}^{N-Q} c_{l+r} \sqrt{\frac{\binom{Q}{l} \binom{N-Q}{r}}{\binom{N}{l+r}}} |D_Q^{(l)}\rangle \otimes |D_{N-Q}^{(r)}\rangle \end{aligned} \quad (\text{B3})$$

The p, q^{th} element of the reduced density matrix, $\rho_Q = \text{tr}_{N-Q} |\psi\rangle \langle \psi|$ is given by:

$$(\rho_Q)_{pq} = \sqrt{\binom{Q}{p} \binom{Q}{q}} \sum_{r=0}^{N-Q} \frac{\binom{N-Q}{r}}{\sqrt{\binom{N}{p+r} \binom{N}{q+r}}} c_{p+r} c_{q+r}^* \quad (\text{B4})$$

Appendix C: More results

In this section, we present the QFI results of more initial states to compare our results with a previous study [66]. The color scheme for the QFI plots for the different initial points is fixed throughout the paper: purple for the equatorial island state $|\pi/2, \pi/2\rangle$, lime-green for island state $|1.82, 1.54\rangle$, blue for non-equatorial island state $|2.20, 2.44\rangle$, red for chaotic sea state $|2.46, 0.32\rangle$ and green for edge state $|2.56, 2.31\rangle$

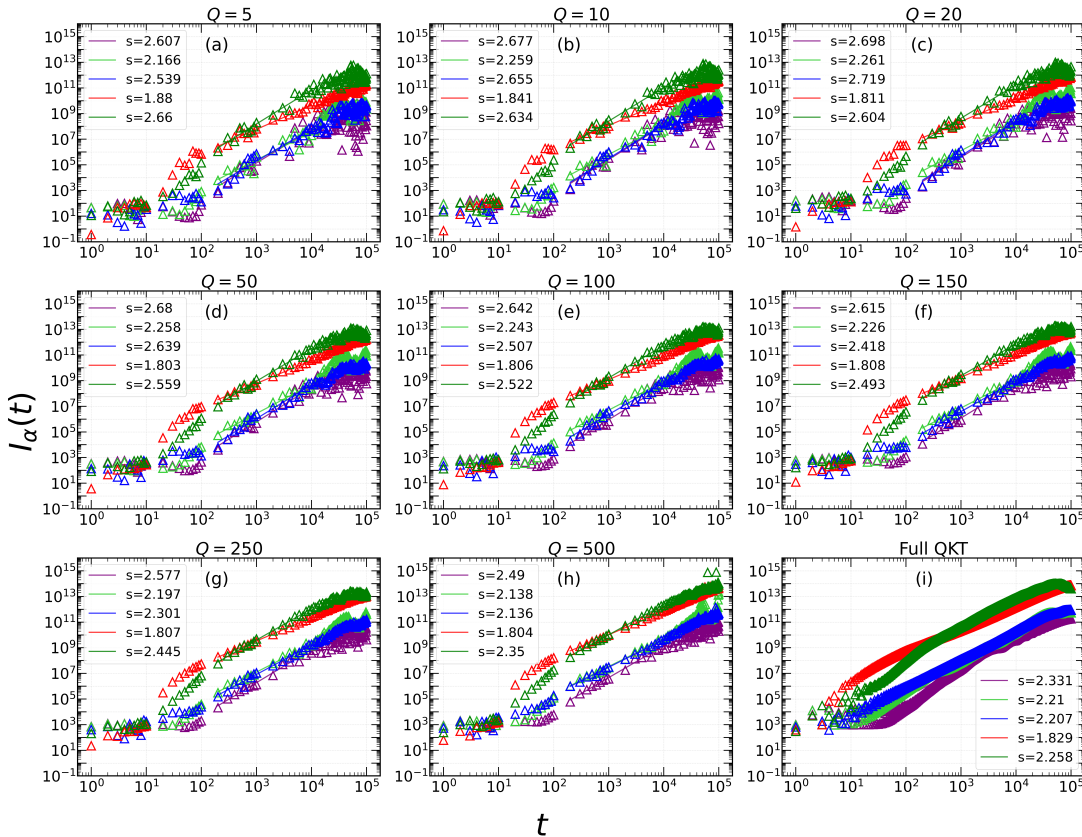


FIG. 7. Scaling of the QFI I_α is presented as a function of time t , for $\kappa = 3.0$ and different subsystem access Q , out of a total of $N = 1000$ qubits. At sufficiently later times, the edge state exhibits the highest QFI, followed closely by the chaotic sea state. Importantly, even in only 5% access, the QFI for the edge state nearly reaches the same order of magnitude as the full access case.

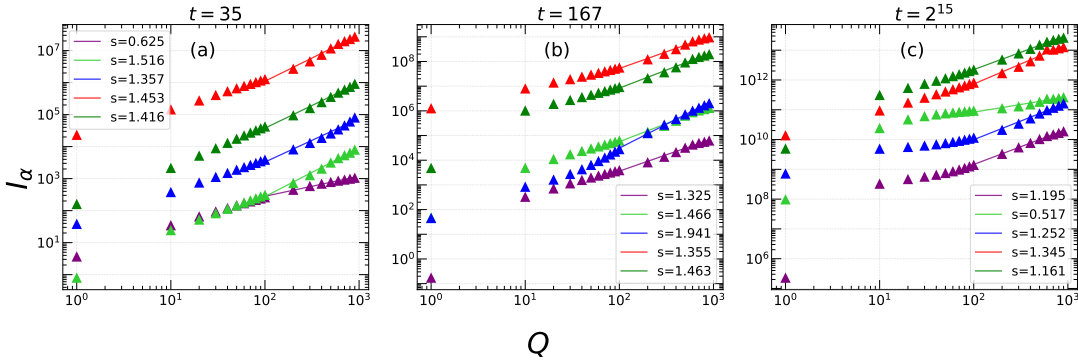


FIG. 8. Scaling of the QFI is shown as a function of the subsystem size Q for $\kappa = 3.0$ and at three different times : (a) $t = t_E = 35$, the Ehrenfest time for the edge state. (b) $t = t_H = 167$, the Heisenberg time of the system. (c) $t = 2^{15}$, a much later time $t \gg t_H$. With time evolution, the separation between the QFI of the initial chaotic and edge states reduces. Eventually, the QFI of the edge state surpasses that of the chaotic state and reaches its highest QFI value. A transition in QFI scaling is observed starting from $Q = 100$. However, at short times, the chaotic initial states provide the larger QFI values and hence the best candidates for sensing

The numerical results of the QFI for different Q is shown in Fig. 7. Among all the initial states, the chaotic state shows the largest QFI value initially but gets surpassed by the edge state at later times. As seen the QFI for different subsystem upto 50% accessibility shows a good scaling with time. Early time behaviour of the QFI is very random, there are fluctuations so the focus should be from the Heisenberg time, t_H . For time $t_H < t \leq 10^4$, the QFI shows quantum enhancement: on average, one can say the scaling is Heisenberg. While the edge state QFI almost reaches the same order as the full top QFI in as low as 5% access at large times, the overall QFI trend for all initial states in 50% access almost mirrors the full access case for $\kappa = 3$.

The QFI scaling with the subsystem size, Q is shown in Fig. 8 for three representative times. Q is varied from 1 to 900 qubits here. The early time and late time behaviour of the different initial states are different. At early times, the chaotic initial state dominates in QFI value but the edge state overcomes it after the Heisenberg time. The QFI scaling with subsystem size, $I_\alpha \sim Q^s$ where $s \simeq [0.625, 1.416]$ at the $t = t_E$. At $t = t_H$, s lies in the range $\simeq [1.325, 1.941]$. At very large time, $t = 2^{15}$, $s \simeq [0.517, 1.345]$. Overall, the QFI dependence on Q can be considered to be linear.

[1] C. R. Rao, Information and the Accuracy Attainable in the Estimation of Statistical Parameters, *Bull. Calcutta Math. Soc* **37**, 81 (1945).

[2] H. Cramér, *Mathematical Methods of Statistics* (Princeton University Press, Princeton, 1946).

[3] R. A. Fisher, On the Mathematical Foundations of Theoretical Statistics, *Phil. Trans. R. Soc.* **222**, 309 (1922).

[4] R. A. Fisher, Theory of Statistical Estimation, *Math. Proc. Camb. Philos. Soc.* **22**, 700–725 (1925).

[5] V. Giovannetti, S. Lloyd, and L. Maccone, Quantum metrology, *Physical Review Letters* **96**, 010401 (2006).

[6] V. Giovannetti, S. Lloyd, and L. Maccone, Advances in quantum metrology, *Nature Photonics* **5**, 222 (2011).

[7] V. Giovannetti, S. Lloyd, and L. Maccone, Quantum-Enhanced Measurements: Beating the Standard Quantum Limit, *Science* **306**, 1330–1336 (2004).

[8] F. Fröwis and W. Dür, Stable Macroscopic Quantum Superpositions, *Phys. Rev. Lett.* **106**, 110402 (2011).

[9] A. N. Boto, P. Kok, D. S. Abrams, S. L. Braunstein, C. P. Williams, and J. P. Dowling, Quantum Interferometric Optical Lithography: Exploiting Entanglement to Beat the Diffraction Limit, *Phys. Rev. Lett.* **85**, 2733 (2000).

[10] J. P. Dowling, Quantum optical metrology – the lowdown on high-N00N states, *Contemp. Phys.* **49**, 125–143 (2008).

[11] J. Joo, W. J. Munro, and T. P. Spiller, Quantum Metrology with Entangled Coherent States, *Phys. Rev. Lett.* **107**, 083601 (2011).

[12] S. Slussarenko, M. M. Weston, H. M. Chrzanowski, L. K. Shalm, V. B. Verma, S. W. Nam, and G. J. Pryde, Unconditional violation of the shot-noise limit in photonic quantum metrology, *Nat. Photonics* **11**, 700–703 (2017).

[13] M. Kitagawa and M. Ueda, Squeezed spin states, *Physical Review A* **47**, 5138 (1993).

[14] D. J. Wineland, J. J. Bollinger, W. M. Itano, F. L. Moore, and D. J. Heinzen, Spin squeezing and reduced quantum noise in spectroscopy, *Phys. Rev. A* **46**, R6797 (1992).

[15] J. Ma and X. Wang, Fisher information and spin squeezing in the Lipkin-Meshkov-Glick model, *Phys. Rev. A* **80**, 012318 (2009).

[16] P. Hyllus, L. Pezzé, and A. Smerzi, Entanglement and Sensitivity in Precision Measurements with States of a Fluctuating Number of Particles, *Phys. Rev. Lett.* **105**, 120501 (2010).

[17] C. Gross, Spin squeezing, entanglement and quantum metrology with Bose-Einstein condensates, *Journal of Physics B: Atomic, Molecular and Optical Physics* **45**, 103001 (2012).

[18] L. A. Rozema, D. H. Mahler, R. Blume-Kohout, and A. M. Steinberg, Optimizing the Choice of Spin-Squeezed States for Detecting and Characterizing Quantum Processes, *Phys. Rev. X* **4**, 041025 (2014).

[19] C. Lyu, S. Choudhury, C. Lv, Y. Yan, and Q. Zhou, Eternal discrete time crystal beating the heisenberg limit, *Physical Review Research* **2**, 033070 (2020).

[20] Z. Zou, J. Gong, and W. Chen, Enhancing quantum metrology by quantum resonance dynamics, *Physical Review Letters* **134**, 230802 (2025).

[21] H. Biswas and S. Choudhury, The floquet central spin model: A platform to realize eternal time crystals, entanglement steering, and multiparameter metrology, arXiv preprint arXiv:2501.18472 (2025).

[22] H. Biswas and S. Choudhury, Discrete time crystals in the spin- s central spin model, arXiv preprint arXiv:2505.13207 (2025).

[23] V. Montenegro, C. Mukhopadhyay, R. Yousefjani, S. Sarkar, U. Mishra, M. G. Paris, and A. Bayat, Quantum metrology and sensing with many-body systems, *Physics Reports* **1134**, 1 (2025).

[24] K. D. Agarwal, S. Mondal, A. Sahoo, D. Rakshit, A. Sen, and U. Sen, Quantum sensing with ultracold simulators in lattice and ensemble systems: A review, *International Journal of Modern Physics C*, 2543006 (2025).

[25] K. Goda, O. Miyakawa, E. E. Mikhailov, S. Saraf, R. Adhikari, K. McKenzie, R. Ward, S. Vass, A. J. Weinstein, and N. Mavalvala, A quantum-enhanced prototype gravitational-wave detector, *Nat. Phys.* **4**, 472–476 (2008).

[26] R. Schnabel, N. Mavalvala, D. E. McClelland, and P. K. Lam, Quantum metrology for gravitational wave astronomy, *Nat. Commun.* **1**, 121 (2010).

[27] J. Aasi, J. Abadie, B. Abbott, R. Abbott, T. Abbott, M. Abernathy, C. Adams, T. Adams, P. Addesso, R. Adhikari, *et al.*, Enhanced sensitivity of the LIGO gravitational wave detector by using squeezed states of light, *Nat. Photonics* **7**, 613 (2013).

[28] S. L. Danilishin, F. Y. Khalili, and H. Miao, Advanced quantum techniques for future gravitational-wave detectors, *Living Rev. Relativ.* **22**, 10.1007/s41114-019-0018-y (2019).

[29] S. D. Bass and M. Doser, Quantum sensing for particle physics, *Nat. Rev. Phys.* **6**, 329 (2024).

[30] V. Giovannetti, S. Lloyd, and L. Maccone, Quantum-enhanced positioning and clock synchronization, *Nature* **412**, 417–419 (2001).

[31] D. F. Jackson Kimball, D. Budker, T. E. Chupp, A. A. Geraci, S. Kolkowitz, J. T. Singh, and A. O. Sushkov, Probing fundamental physics with spin-based quantum sensors, *Phys. Rev. A* **108**, 010101 (2023).

[32] D. DeMille, N. R. Hutzler, A. M. Rey, and T. Zelevinsky, Quantum sensing and metrology for fundamental physics with molecules, *Nat. Phys.* **20**, 741–749 (2024).

[33] R. Kaubruegger and A. M. Kaufman, Progress in quantum metrology and applications for optical atomic clocks, arXiv preprint arXiv:2512.02202 (2025).

[34] I. Baumgart, J.-M. Cai, A. Retzker, M. B. Plenio, and C. Wunderlich, Ultrasensitive Magnetometer using a Single Atom, *Phys. Rev. Lett.* **116**, 240801 (2016).

[35] U. Mishra and A. Bayat, Integrable quantum many-body sensors for AC field sensing, *Sci. Rep.* **12**, 10.1038/s41598-022-17381-y (2022).

[36] H. Zhou, J. Choi, S. Choi, R. Landig, A. M. Douglas, J. Isoya, F. Jelezko, S. Onoda, H. Sumiya, P. Cappellaro, H. S. Knowles, H. Park, and M. D. Lukin, Quantum Metrology with Strongly Interacting Spin Systems, *Phys. Rev. X* **10**, 031003 (2020).

[37] G. Tóth and I. Apellaniz, Quantum metrology from a quantum information science perspective, *Journal of Physics A: Mathematical and Theoretical* **47**, 424006 (2014).

[38] A. Luis, Nonlinear transformations and the Heisenberg limit, *Phys. Lett. A* **329**, 8 (2004).

[39] J. Beltrán and A. Luis, Breaking the Heisenberg limit with inefficient detectors, *Phys. Rev. A* **72**, 045801 (2005).

[40] A. Luis, Quantum limits, nonseparable transformations, and nonlinear optics, *Phys. Rev. A* **76**, 035801 (2007).

[41] S. Boixo, S. T. Flammia, C. M. Caves, and J. Geremia, Generalized Limits for Single-Parameter Quantum Estimation, *Phys. Rev. Lett.* **98**, 090401 (2007).

[42] S. Boixo, A. Datta, M. J. Davis, S. T. Flammia, A. Shaji, and C. M. Caves, Quantum Metrology: Dynamics versus Entanglement, *Phys. Rev. Lett.* **101**, 040403 (2008).

[43] M. Beau and A. del Campo, Nonlinear Quantum Metrology of Many-Body Open Systems, *Phys. Rev. Lett.* **119**, 010403 (2017).

[44] J. Yang, S. Pang, A. del Campo, and A. N. Jordan, Super-Heisenberg scaling in Hamiltonian parameter estimation in the long-range Kitaev chain, *Phys. Rev. Res.* **4**, 013133 (2022).

[45] S. M. Roy and S. L. Braunstein, Exponentially Enhanced Quantum Metrology, *Phys. Rev. Lett.* **100**, 220501 (2008).

[46] L. Pezzé and A. Smerzi, Entanglement, Nonlinear Dynamics, and the Heisenberg Limit, *Phys. Rev. Lett.* **102**, 100401 (2009).

[47] P. Zanardi and N. Paunković, Ground state overlap and quantum phase transitions, *Phys. Rev. E* **74**, 031123 (2006).

[48] C. Invernizzi, M. Korbman, L. Campos Venuti, and M. G. A. Paris, Optimal quantum estimation in spin systems at criticality, *Phys. Rev. A* **78**, 042106 (2008).

[49] S. Gammelmark and K. Mølmer, Phase transitions and heisenberg limited metrology in an ising chain interacting with a single-mode cavity field, *New J. Phys.* **13**, 053035 (2011).

[50] M. Skotiniotis, P. Sekatski, and W. Dür, Quantum metrology for the Ising Hamiltonian with transverse magnetic field, *New J. Phys.* **17**, 073032 (2015).

[51] M. M. Rams, P. Sierant, O. Dutta, P. Horodecki, and J. Zrazewski, At the Limits of Criticality-Based Quantum Metrology: Apparent Super-Heisenberg Scaling Revisited, *Phys. Rev. X* **8**, 021022 (2018).

[52] Y. Chu, S. Zhang, B. Yu, and J. Cai, Dynamic Framework for Criticality-Enhanced Quantum Sensing, *Phys. Rev. Lett.* **126**, 010502 (2021).

[53] R. Di Candia, F. Minganti, K. V. Petrovni, G. S. Paraoanu, and S. Felicetti, Critical parametric quantum sensing, *npj Quantum Inf.* **9**, 10.1038/s41534-023-00690-z (2023).

[54] S. Yin, J. Song, Y. Zhang, and S. Liu, Quantum Fisher information in quantum critical systems with topological characterization, *Phys. Rev. B* **100**, 184417 (2019).

[55] Y.-R. Zhang, Y. Zeng, T. Liu, H. Fan, J. Q. You, and F. Nori, Multipartite entanglement of the topologically ordered state in a perturbed toric code, *Phys. Rev. Res.* **4**, 023144 (2022).

[56] P. Zanardi, M. G. A. Paris, and L. Campos Venuti, Quantum criticality as a resource for quantum estimation, *Phys. Rev. A* **78**, 042105 (2008).

[57] I. Frerot and T. Roscilde, Quantum Critical Metrology, *Phys. Rev. Lett.* **121**, 020402 (2018).

[58] C. Hotter, H. Ritsch, and K. Gietka, Combining Critical and Quantum Metrology, *Phys. Rev. Lett.* **132**, 060801 (2024).

[59] E. Davis, G. Bentsen, and M. Schleier-Smith, Approaching the heisenberg limit without single-particle detection, *Physical review letters* **116**, 053601 (2016).

[60] D. Braun, G. Adesso, F. Benatti, R. Floreanini, U. Marzolini, M. W. Mitchell, and S. Pirandola, Quantum-enhanced measurements without entanglement, *Rev. Mod. Phys.* **90**, 035006 (2018).

[61] W. Liu, M. Zhuang, B. Zhu, J. Huang, and C. Lee, Quantum metrology via chaos in a driven Bose-Josephson system, *Phys. Rev. A* **103**, 023309 (2021).

[62] Z. Li, S. Colombo, C. Shu, G. Velez, S. Pilatowsky-Cameo, R. Schmied, S. Choi, M. Lukin, E. Pedrozo-Peñafield, and V. Vuletić, Improving metrology with quantum scrambling, *Sci-*

ence **380**, 1381 (2023).

[63] B. Kobrin, T. Schuster, M. Block, W. Wu, B. Mitchell, E. Davis, and N. Y. Yao, A universal protocol for quantum-enhanced sensing via information scrambling, arXiv preprint arXiv:2411.12794 (2024).

[64] G. Hu, W. Zhang, Z. Chen, L. Zhong, J. Zhao, C. Liu, Z. Liu, Y. Xu, Y. Lin, Y. Ri, *et al.*, Quantum-enhanced sensing enabled by scrambling-induced genuine multipartite entanglement, arXiv preprint arXiv:2601.22503 (2026).

[65] V. Montenegro, S. Dornetti, A. Ferraro, and M. G. Paris, Enhanced quantum frequency estimation by nonlinear scrambling, *Physical Review Letters* **135**, 030802 (2025).

[66] L. J. Fiderer and D. Braun, Quantum metrology with quantum-chaotic sensors, *Nat. Commun.* **9**, 1351 (2018).

[67] H.-L. Shi, A. Smerzi, and L. Pezzè, Quantum chaos, randomness and universal scaling of entanglement in various krylov spaces, *SciPost Physics* **19**, 102 (2025).

[68] J. Schuff, L. J. Fiderer, and D. Braun, Improving the dynamics of quantum sensors with reinforcement learning, *New Journal of Physics* **22**, 035001 (2020).

[69] S. Asthana, Y. Ibrahim, N. T. W. Koo, and S. Vinjanampathy, Projected optimal sensors from operator orbits, arXiv preprint arXiv:2512.13294 (2025).

[70] U. Mishra and A. Bayat, Driving Enhanced Quantum Sensing in Partially Accessible Many-Body Systems, *Phys. Rev. Lett.* **127**, 080504 (2021).

[71] M. Adani, S. Cavazzoni, B. Teklu, P. Bordone, and M. G. A. Paris, Critical metrology of minimally accessible anisotropic spin chains, *Sci. Rep.* **14**, 10.1038/s41598-024-70307-8 (2024).

[72] Q.-K. Wan, H.-L. Shi, and X.-W. Guan, Quantum-enhanced metrology in cavity magnonics, *Phys. Rev. B* **109**, L041301 (2024).

[73] V. Montenegro, Heisenberg-limited spin-mechanical gravimetry, *Phys. Rev. Res.* **7**, 013016 (2025).

[74] J. Li, D. Cui, and X. X. Yi, Parameter estimation with limited access to measurements, *Phys. Rev. A* **109**, 032215 (2024).

[75] F. Haake, M. Kuś, and R. Scharf, Classical and quantum chaos for a kicked top, *Z. Physik B - Condensed Matter* **65**, 381–395 (1987).

[76] A. Piga, M. Lewenstein, and J. Q. Quach, Quantum chaos and entanglement in ergodic and nonergodic systems, *Phys. Rev. E* **99**, 032213 (2019).

[77] S. L. Braunstein and C. M. Caves, Statistical distance and the geometry of quantum states, *Phys. Rev. Lett.* **72**, 3439 (1994).

[78] S. L. Braunstein, C. M. Caves, and G. Milburn, Generalized Uncertainty Relations: Theory, Examples, and Lorentz Invariance, *Ann. Phys.* **247**, 135 (1996).

[79] M. G. A. Paris, Quantum estimation for quantum technology, *Int. J. Quantum Inf.* **07**, 125 (2009).

[80] C. Helstrom, Minimum mean-squared error of estimates in quantum statistics, *Phys. Lett. A* **25**, 101 (1967).

[81] C. W. Helstrom, Quantum detection and estimation theory, *J. Stat. Phys.* **1**, 231–252 (1969).

[82] A. S. Holevo, *Probabilistic and Statistical Aspects of Quantum Theory*, North-Holland Series in Statistics and Probability, Vol. 1 (North-Holland Publishing Company, Amsterdam, 1982).

[83] P. Hyllus, W. Laskowski, R. Krischek, C. Schwemmer, W. Wieczorek, H. Weinfurter, L. Pezzè, and A. Smerzi, Fisher information and multiparticle entanglement, *Phys. Rev. A* **85**, 022321 (2012).

[84] G. Tóth, Multiparticle entanglement and high-precision metrology, *Phys. Rev. A* **85**, 022322 (2012).

[85] K. Gietka, J. Chwedeńczuk, T. Wasak, and F. Piazza, Multi-partite entanglement dynamics in a regular-to-ergodic transition: Quantum Fisher information approach, *Phys. Rev. B* **99**, 064303 (2019).

[86] T.-L. Wang, L.-N. Wu, W. Yang, G.-R. Jin, N. Lambert, and F. Nori, Quantum Fisher information as a signature of the superradiant quantum phase transition, *New J. Phys.* **16**, 063039 (2014).

[87] P. M. Poggi and M. H. Muñoz-Arias, Measurement-induced multipartite-entanglement regimes in collective spin systems, *Quantum* **8**, 1229 (2024).

[88] N. Chakrabarti, N. Nirbhan, and A. Bhattacharyya, Dynamics of monitored SSH model in Krylov space: from complexity to quantum Fisher information, *J. High Energy Phys.* **2025** (7).

[89] J. M. Radcliffe, Some properties of coherent spin states, *J. Phys.* **4**, 313 (1971).

[90] F. T. Arecchi, E. Courtens, R. Gilmore, and H. Thomas, Atomic Coherent States in Quantum Optics, *Phys. Rev. A* **6**, 2211 (1972).

[91] F. Haake, S. Gnutzmann, and M. Kuś, *Quantum Signatures of Chaos*, Springer Series in Synergetics (Springer International Publishing, Cham, 2018).

[92] C. Neill, P. Roushan, M. Fang, Y. Chen, M. Kolodrubetz, Z. Chen, A. Megrant, R. Barends, B. Campbell, B. Chiaro, *et al.*, Ergodic dynamics and thermalization in an isolated quantum system, *Nature Physics* **12**, 1037 (2016).

[93] S. Chaudhury, A. Smith, B. Anderson, S. Ghose, and P. S. Jessen, Quantum signatures of chaos in a kicked top, *Nature* **461**, 768 (2009).

[94] V. Krishika, V. Anjusha, U. T. Bhosale, and T. Mahesh, Nmr studies of quantum chaos in a two-qubit kicked top, *Physical Review E* **99**, 032219 (2019).

[95] J. I. Latorre, R. Orús, E. Rico, and J. Vidal, Entanglement entropy in the Lipkin-Meshkov-Glick model, *Phys. Rev. A* **71**, 064101 (2005).

[96] R. I. Nepomechie, F. Ravanini, and D. Raveh, Spin-ss Dicke States and Their Preparation, *Adv. Quantum Technol.* **7**, 10.1002/quate.202400057 (2024).